Structural and Photomagnetic Studies of Two Compounds in the System $Cu^{2+}/Mo(CN)_8^{4-}$: From Trinuclear Molecule to Infinite Network†

Guillaume Rombaut,‡ Marc Verelst,§ Stéphane Golhen,|| Lahcène Ouahab,|| Corine Mathonière,*,‡ and Olivier Kahn†,‡

Laboratoire des Sciences Moléculaires, Institut de Chimie de la Matière Condensée de Bordeaux, UPR CNRS No. 9048, 33608 Pessac Cedex, France, Centre d'Elaboration de Matériaux et d'Etudes Structurales, UPR CNRS No. 8011, BP 4743, 29 Rue Jeanne Marvig, 31055 Toulouse, France, and Laboratoire de Chimie du Solide et Inorganique Moléculaire, UMR 6511 CNRS−Université de Rennes 1, Institut de Chimie de Rennes, Avenue du Général Leclerc, 35042 Rennes Cedex, France

Received August 4, 2000

The syntheses and structural and physical characterization of the compounds $[Cu(bipy)_2]_2[Mo(CN)_8]\cdot 5H_2O\cdot CH_3OH$ (**1**) with bipy = 2,2′-bipyridine and $M^{II}_2[Mo^{IV}(CN)_8]\cdot xH_2O$ (**2** with M = Cu, $x = 7.5$; **3** with M = Mn, $x = 9.5$) are presented. **1** crystallizes in the triclinic space group $P\bar{1}$ ($a = 11.3006(4)$ Å, $b = 12.0886(5)$ Å, $c = 22.9589(9)$ Å, $\alpha = 81.799(2)°$, $\beta = 79.787(2)°$, $\gamma = 62.873(2)°$, $Z = 2$). The structure of **1** consists of neutral trinuclear molecules in which a central $[Mo(CN)_8]^{4-}$ anion is linked to two $[Cu(bipy)_2]^{2+}$ cations through two cyanide bridges. **2** crystallizes poorly, and hence, structural information has been obtained from the wide-angle X-ray scattering (WAXS) technique, by comparison with **3** and $Fe^{II}_2(H_2O)_4[Mo^{IV}(CN)_8]\cdot 4H_2O$ whose X-ray structure has been previously solved. **2**, **3**, and $Fe^{II}_2(H_2O)_4[Mo^{IV}(CN)_8]\cdot 4H_2O$ form extended networks with all the cyano groups acting as bridges. The magnetic properties have shown that **1** and **2** behave as paramagnets. Under irradiation with light, they exhibit important modifications of their magnetic properties, with the appearance at low temperature of magnetic interactions. For **1** the modifications are irreversible, whereas they are reversible for **2** after cycling in temperature. These photomagnetic effects are thought to be caused by the conversion of Mo^{IV} (diamagnetic) to Mo^{V}(paramagnetic) through a photooxidation mechanism for **1** and a photoinduced electron transfer in **2**. These results have been correlated with the structural features.

Introduction

In 1996, a new area in the field of molecular magnetism opened following the discovery by Hashimoto and co-workers of photoinduced long-range magnetic ordering in a Prussian blue analogue.[1] This photomagnetic effect is of considerable importance because the control of magnetic properties by external stimuli has been demonstrated in molecular materials for the first time. The Prussian blue analogue of interest is obtained from aqueous solutions of hexacyanoferrate(III) and Co^{II}, leading to a compound formulated as $K_{0.2}Co_{1.4}[Fe(CN)_6]\cdot 6.9H_2O$. The formula hides a subtle chemical composition with many $Fe^{III}-CN-Co^{II}$ units and a minority of $Fe^{II}-CN-Co^{III}$ arising from an internal redox reaction and also vacancies filled with water molecules in a face-centered cubic structure. This compound behaves as a ferrimagnet with a long-range magnetic ordering temperature $T_c = 16$ K. After irradiation with red light corresponding to a metal−metal charge-transfer band, the magnetization is enhanced and the Curie temperature is increased to 19 K. The return to the initial state has been obtained by irradiation with blue light or thermal treatment, showing the reversibility of the phenomenon. This effect has been explained by a photoinduced electron transfer from Fe^{II} to Co^{III} through the cyanide bridge in isolated diamagnetic pairs Fe^{II}(low spin $S = 0$)$-Co^{III}$(low spin $S = 0$), leading to magnetic pairs Fe^{III}(low spin $S = {}^1/_2$)$-Co^{II}$(high spin $S = {}^3/_2$). The photoinduced magnetization is due to the increase of the number of magnetic pairs in the material. More recently, new related materials have been described with rubidium instead of potassium ion.[2] These compounds contain around 80% diamagnetic $Fe^{II}-Co^{III}$ pairs and around 20% Co^{II}. Their magnetic behavior is expected for isolated paramagnetic Co^{II} ions. After irradiation, these materials become ferrimagnets at 22 K. These compounds exhibit the most intense photomagnetic effects reported so far, passing over from the paramagnetic regime to ferrimagnetic ordering. In contrast, the compound $KCo^{III}[Fe^{II}(CN)_6]$ without any vacancy exhibits no, or a very small photomagnetic, effect.[3] These results show that the conditions required to observe the photomagnetic effect are not only the presence of diamagnetic excitable pairs but also the presence of defects in the cubic structure. The control of these two conditions remains a challenge for the chemist.

A different chemical strategy is the preparation of photomagnetic extended systems using light-sensitive coordination compounds as building blocks. The choice of the precursors is

† This paper is dedicated to the memory of Olivier Kahn who died on December 8, 1999.

‡ Institut de Chimie de la Matière Condensée de Bordeaux.

§ Centre d'Elaboration de Matériaux et d'Etudes Structurales.

|| Institut de Chimie de Rennes.

(1) (a) Sato, O.; Iyoda, T.; Fujishima, A.; Hashimoto, K. *Science* **1996**, *272*, 49. (b) Verdaguer, M. *Science* **1996**, *272*, 698.

(2) (a) Verdaguer, M.; Bleuzen, A.; Marvaud, V.; Vaissermann, J.; Seuleiman, J.; Desplanches, C.; Scuiller, A.; Train, C.; Garde, R.; Gelly, G.; Lomenech, C.; Rosenman, I.; Veilet, P.; Cartier, C.; Villain, F. *Coord. Chem. Rev.* **1999**, *190−192*, 1023. (b) Sato, O.; Einaga, Y.; Fujishima, A.; Hashimoto, K. *Inorg. Chem.* **1999**, *38*, 4405. (c) Goujon, A.; Roubeau, O.; Varret, F.; Dolbecq, A.; Bleuzen, A.; Verdaguer, M. *Eur. Phys. J. B* **2000**, *14*, 115.

(3) Hashimoto, H.; Ohkoshi, S.-H. *Philos. Trans. R. Soc. London* **1999**, *357*, 2977.

10.1021/ic0008722 CCC: $20.00
Published on Web 02/07/2001

guided by two criteria: (i) their photoreactions must implicate a change in spin state; (ii) the presence of bridging ligands. In this context, Hashimoto's group proposed the construction of a switchable spin device obtained with the photochromic anion $[Fe^{II}(CN)_5NO]^{2-}$. However, the solid obtained, $Ni^{II}[Fe^{II}(CN)_5NO]\cdot 5H_2O$, exhibited a weak enhancement of the magnetization.[4] The octacyanometalate of formula $K_4[Mo^{IV}(CN)_8]\cdot 2H_2O$ is a good candidate for our purpose. First, the solution photochemistry of this compound has been studied for many years. In particular, the irradiation with light of a solution containing $[Mo^{IV}(CN)_8]^{4-}$ in its charge-transfer bands results in a photooxidation of $Mo^{IV}(S = 0)$ in $Mo^{V}(S = {}^1/_2)$ with the ejection of a solvated electron.[5] We recently checked that this property is maintained in the solid state.[6] Second, the ability of cyanometalates to form compounds with several metallic centers is well-established.[2a,7] In this way, we have recently shown that in a bimetallic chain formed by Mn^{II}(mac), mac being a macrocycle ligand, and $Mo^{IV}(CN)_8{}^{4-}$, the photooxidation process is still operative, leading in this case to the formation after light irradiation to ferrimagnetic chains.[6]

In the general framework of the study of electron-transfer reactions, most of the studies done on the octacyanometalates have focused on ion-paired assemblies in solution. Moreover, because of its diamagnetic ground state, the $Mo^{IV}(CN)_8{}^{4-}$ precursor has not yet been considered as the building block of extended magnetic networks. In this work, we show that it can be used for the preparation of magnetic compounds, reacting to the light irradiation through photooxidation and electron-transfer processes.

In 1984, Henning's group studied the electron transfer in $M^{n+}/Mo^{IV}(CN)_8{}^{4-}$ systems, M being a transition metal.[8] The $Cu^{2+}/Mo^{IV}(CN)_8{}^{4-}$ system is particularly interesting for our purpose because an intense intervalence transfer band has been identified in the visible range. This encouraged us to prepare compounds containing both Cu^{2+} and $Mo^{IV}(CN)_8$ units. Syntheses of compounds with formula $M^{II}_2[Mo^{IV}(CN)_8]\cdot xH_2O$ have been already described by McKnight et al.[9] We reinvestigated these compounds with M = Mn, Fe, and Cu to explore in detail their structural, magnetic, and photomagnetic properties. For M = Fe only, we succeeded in obtaining well-shaped crystals. The X-ray structure and magnetic properties of the compound $Fe^{II}_2(H_2O)_4[Mo^{IV}(CN)_8]\cdot 4H_2O$ have been reported elsewhere.[10] The compound crystallizes in the tetragonal space group $I\bar{4}22$, with $a = 11.809(2)$ Å and $c = 13.108(2)$ Å. The structure consists of an extended network of alternating $Mo(CN)_8$ and $Fe(H_2O)_2$ units, and the three-dimensional architecture is formed by two perpendicular grids (Figure 1). The Mo ion surrounded by eight cyanide groups has been described as a square antiprism, whereas the Fe ion is in an octahedral environment formed by four CN groups and two water molecules in apical positions. In this paper, we focused on the Cu and Mn phases (noted as **2** and **3**) prepared as powders. Only the Cu phase exhibits photomagnetic effects when irradiated in intervalence or ligand-field bands. In addition to these extended networks, we prepared single crystals of a new compound constituted by trinuclear molecules of formula $[Cu(bipy)_2]_2[Mo(CN)_8]\cdot 5H_2O\cdot CH_3OH$ (noted as **1**) where the ligand bipy (=2,2′-bipyridine) was used for blocking coordination sites around the Cu ion. In the following, the structural characterization of the compounds, using X-ray analysis for **1** and a wide-angle X-ray scattering study of **2** and **3**, is reported. Finally the magnetic and photomagnetic properties will be presented. Then the results obtained for both compounds will be compared and discussed.

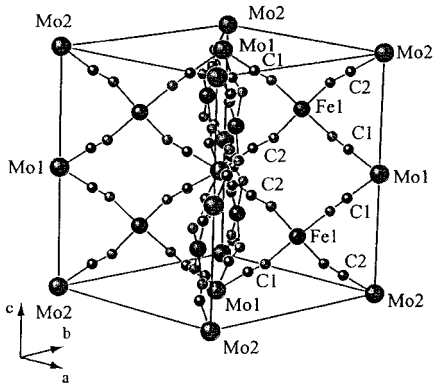

Figure 1. Structure of the $Fe^{II}_2(H_2O)_4[Mo^{IV}(CN)_8]\cdot 4H_2O$ compound.

Experimental Section

Synthesis and Physical Characterization. Details of the syntheses of $K_4[Mo(CN)_8]\cdot 2H_2O$ and $M^{II}_2[Mo^{IV}(CN)_8]\cdot xH_2O$, with M = Cu (**2**), Mn (**3**), are given elsewhere.[11,9]

$[Cu(bipy)_2]_2[Mo(CN)_8]\cdot 5H_2O\cdot CH_3OH$ (1). Light-green single crystals suitable for X-ray analysis were obtained in a test tube by slow diffusion of the upper methanolic solution containing both bipyridine and $Cu(SO_4)_2$ into the lower aqueous solution of $K_4[Mo(CN)_8]\cdot 2H_2O$. IR spectra (KBr pellet, selected bands ν/cm^{-1}): 3421 (O−H stretching), 2124 and 2112 (C−N stretching), 1600, 1445, and 772 (bipy C=C stretching and C−H bending). UV−vis spectra (KBr pellet, λ/nm): 680 nm (Cu ligand field transitions), 420 nm (shoulder, Mo ligand field transition).

$M_2[Mo(CN)_8]\cdot xH_2O$ (M = Cu (2) with $x = 7.5$, M = Mn (3) with $x = 9.5$). These compounds were prepared as powders. All our attempts to obtain single crystals were unsuccessful. Anal. Calcd for **2**: C, 19.27; N, 19.65; H, 2.30; Cu, 22.45; Mo, 17.03. Found: C, 16.97; N, 19.79; H, 2.67; Cu, 22.44; Mo, 16.94. IR spectra (KBr pellet, selected bands ν/cm^{-1}): 3421 (O−H stretching), 2161 (C−N stretching), 445 and 422 (M−C stretching and M-CN bending). UV−vis spectra (KBr pellet, λ/nm): 730 nm (Cu ligand field transitions), 520 nm (intervalence charge-transfer $Cu^{II}-Mo^{IV} \rightarrow Cu^{I}-Mo^{V}$), 380 nm (shoulder, Mo ligand-field transition). Anal. Calcd for **3**: C, 16.42; N, 19.15; Mn, 18.78; Mo, 16.40. Found: C, 17.65; N, 19.20; Mn, 18.85; Mo, 16.65. IR spectra (KBr pellet, selected ν/cm^{-1}): 3450 (O−H stretch), 2131 (C−N stretch), 447 and 419 (M−C stretching and M−CN bending). UV−vis spectra (KBr pellet, λ/nm): 430 and 375 nm (Mo ligand field transitions).

Crystallographic Data Collection and Structure Determination. A single crystal was mounted on a Nonius Kappa CCD area-detector diffractometer equipped with a graphite-monochromatized molybdenum Kα radiation ($\lambda = 0.710\,73$ Å). A total of 15 533 unique reflections

(4) (a) Gu, Z.; Sato, O.; Iyoda, T.; Hashimoto, K.; Fujishima, A. *J. Phys. Chem.* **1996**, *47*, 18290. (b) Gu, Z.; Sato, O.; Iyoda, T.; Hashimoto, K.; Fujishima, A. *Chem. Mater.* **1997**, *9*, 1092.
(5) (a) Waltz, W. L.; Adamson, A. W *J. Phys. Chem.* **1969**, *73*, 4250. (b) Waltz, W. L.; Adamson, A. W; Fleischauer, P. D. *J. Am. Chem. Soc.* **1967**, *89*, 3923. (c)Shirom, M.; Siderer, Y. *J. Chem. Phys.* **1972**, *57*, 1013 (d) Shirom, M.; Siderer, Y. *J. Chem. Phys.* **1973**, *58*, 1250. (e) Vogler, A.; Losse, W.; Kunkely, H. *J. Chem. Soc., Chem. Commun.* **1979**, 187. (f) Bettelheim, A.; Shirom, M. *Chem. Phys. Lett.* **1971**, *9*, 166.
(6) Rombaut, G.; Golhen, S.; Ouahab, L.; Mathonière, C.; Kahn, O. *J. Chem. Soc., Dalton Trans.* **2000**, 3609.
(7) For reviews see, for example, the following. (a) Griffith, W. P. *Chem. Rev.* **1975**, *17*, 177. (b) Sharpe, A. G. *The Chemistry of Cyano Complexes of the Transition Metals*; Academic Press: London, 1976. (c) Dunbar, K. R.; Heintz, R. A. *Prog. Inorg. Chem.*, **1997**, *45*, 283.
(8) Henning, H.; Rehorek, A.; Rehorek, D.; Thomas, P. *Inorg. Chim. Acta* **1984**, *86*, 41.
(9) McKnight, G. F.; Haight, G. P., Jr. *Inorg. Chem.* **1973**, *12*, 3007.
(10) Sra, A. K.; Rombaut, G.; Lahitête, F.; Golhen, S.; Ouahab, L.; Mathonière, C.; Yakhmi, J. V.; Kahn, O. *New. J. Chem.* **2000**, *24*, 871.
(11) Leipoldt, J. D.; Bok, C.; Cilliers, P. J. *Z. Anorg. Allg. Chem.* **1974**, *409*, 343.

Table 1. Crystal Parameters and X-ray Diffraction Data for **1**

chemical formula	$C_{49}H_{46}Cu_2MoN_{16}O_6$
fw	1178.04
temp, K	293(2)
λ, Å	0.710 73
space group	$P\bar{1}$
a, Å	11.3006(4)
b, Å	12.0886(5)
c, Å	22.9589(9)
α, deg	81.799(2)
β, deg	79.787(2)
γ, deg	62.873(2)
V, Å^3	2740.31(18)
Z	2
ρ_{obsd}, g cm^{-3}	1.428
μ, mm^{-1}	1.055
$R\ [I \geq 2\sigma(I)]^a$	0.0788 [9839]
wR2^b	0.2055

^{a} $R = \sum||F_o| - |F_c||/\sum|F_o|$. ^{b} $wR2 = \{\sum[w(F_o^2 - F_c^2)^2]/\sum[w(F_o^2)^2]\}^{1/2}$.

were collected (R_{int} = 3.5%). For data reduction and cell refinement the programs DENZO and SCALEPACK were applied.[12] The structure was solved by direct methods using SHELXS-97 and refined with SHELXL-97 programs by full-matrix least-squares method, on F^2.[13] The crystal data are summarized in Table 1. All non-hydrogen atoms were refined anisotropically. An isotropic thermal parameter 1.2 or 1.5 times that of the parent atom was assigned to hydrogen atoms, which were allowed to ride.

Wide-Angle X-ray Scattering (WAXS) Study. Powders of **2** and **3** were sealed in a Lindemann capillary. The scattering diffusion spectrum of the samples irradiated with graphite-monochromatized molybdenum Kα radiation (λ = 0.710 69 Å) was obtained using a LASIP diffractometer.[14] A total of 457 intensities corresponding to equidistant points ($s = 4\pi[\sin(\theta/\lambda)]$; Δs = 0.035 Å^{-1}) were collected in the range $0 < \theta < 65°$. Immediately afterward, measurements of air and Lindemann capillary diffusion were done under exactly the same conditions. The scattered intensity (sample + air + capillary) of the raw sample was corrected for air and capillary contributions by spectral subtraction, taking into account absorption from the sample, and then corrected for polarization and self-absorption effects. Normalization was performed using Norman and Krogh-Moe's method.[15] The atomic scattering factors were taken from Cromer and Waber.[16] The reduced experimental radial distribution function (RDF) was calculated similarly as given in ref 17. Theoretical structural models were built up using the CERIUS2 program,[18] starting from the reported structure given for $Fe^{II}_2(H_2O)_4[Mo^{IV}(CN)_8]\cdot 4H_2O$.[10] The theoretical RDF was computed from the structural models by Fourier transform of the theoretical intensities calculated using the Debye's formula.[19]

Magnetic and Photomagnetic Studies. These experiments were carried out with a Quantum Design MPMS-5S magnetometer working in the dc mode. The measurements were performed in the 2−300 K range with a magnetic field of 1000 Oe. The photomagnetic experiments were performed with a Kr^+ laser coupled through an optical fiber directed into the superconducting quantum interference device (SQUID) cavity. Crystalline and powdered samples of **1** and **2**, respectively, were laid down on a diamagnetic sample holder (calibrated) as thin layers (weight, ca. 0.3 mg) to avoid surface effects during illumination. The exact weight was estimated by comparing the magnetization curve at 10 K before irradiation with the curve recorded in a routine magnetic experiment (20 mg of sample loaded into gel caps). The samples were irradiated continuously using a multiline at 337 and 356 nm in the UV range or a single line at 480 nm in the visible range under a magnetic field of 10 kOe at 10 K. Magnetic properties were recorded before and after irradiation, in each case the light being turned off to avoid thermal inhomogeneities. Because of the small quantity of matter, the uncertainties of the experimental points above 200 K become important and we limit ourselves to represent the magnetic data after irradiation in the 2−200 K range.

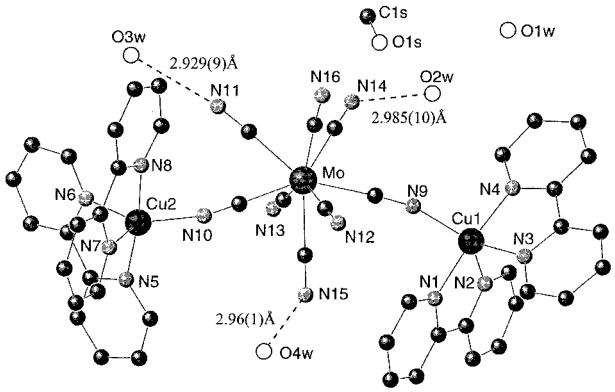

Figure 2. Structure of $[Cu(bipy)_2]_2[Mo(CN)_8]\cdot 5H_2O\cdot CH_3OH$ (**1**).

Results

Structure of $[Cu(bipy)_2]_2[Mo(CN)_8]\cdot 5H_2O\cdot CH_3OH$ (1). The compound crystallizes in the $P\bar{1}$ space group and contains three metal sites: one molybdenum site and two copper sites. All the atoms are localized in the general positions. Figure 2 shows an ORTEP representation of the molecule. It consists of one octacyanomolybdate $Mo(CN)_8$ fragment coordinated via two cyano bridges to two $Cu(bipy)_2$ fragments, the six other cyano groups being terminal. The Mo atom is coordinated by eight CN groups at the corner of an irregular dodecahedron with Mo−C distances ranging from 2.136(5) to 2.178(5) Å. Each Cu sphere may be described as a distorded trigonal bipyramidal geometry with axial and equatorial ligands, the axial atoms being N1 and N4 for Cu1 and N5 and N8 for Cu2. The $Cu-N_{ax}$ distances are homogeneous with an average value of 1.990 Å, but the $Cu-N_{eq}$ distances are in the 1.963−2.153 Å range for both copper spheres. The Mo−C−N angles deviate from linearity with angles ranging from 175.4(5)° to 178.1(4)°, whereas Cu1−N9−C41 and Cu2−N10−C42 angles are 161.3(4) and 166.6(5)°, respectively. The intramolecular distances Mo1−Cu1, Mo1−Cu2, and Cu1−Cu2 are equal to 5.1625(7), 5.2325(8), and 9.795(1) Å, respectively, with an angle Cu2−Mo1−Cu1 of 140.87(1)°. The two bipyridine fragments linked to Cu1 form an angle of 82.1(1)° between them, whereas those linked to Cu2 form an angle of 83.3(1)°. All the $[Cu(bipy)_2]_2[Mo(CN)_8]$ molecules are isolated in the structure, the shortest intermolecular distance between one carbon atom and one hydrogen atom of N15−H34 being 2.435 Å and the shortest distance excluding hydrogen atoms being 3.292(9) Å. The structure contains five water molecules and one methanol molecule per $[Cu(bipy)_2]_2[Mo(CN)_8]$ fragment. All oxygen atoms, except O5w, interact with free cyano fragments with N−O distances shorter than 3 Å (see Table 2). These short

(12) Otwinowski, Z.; Minor, W. *Processing of X-Ray Diffraction Data Collected in Oscillation Mode*; Academic Press: New York, 1996.
(13) Sheldrick, G. M. *SHELXL 97, Program for the Refinement of Crystal Structures*; University of Göttingen: Göttingen, Germany.
(14) The LASIP diffractometer has a geometry especially set up for scattering measurements. It minimizes every external parasite scattering phenomenon.
(15) (a) Norman, N. *Acta Crystallogr*. **1957**, *10*, 370. (b) Krogh-Moe, *Acta Crystallogr*. **1956**, *9*, 951.
(16) Cromer, D.; Waber, T. J. *International Tables for X-ray Crystallography*: Kynoch Press: Birmingham, 1974; Vol. 4.
(17) (a) Mosset, A.; Lecante, P.; Galy, J. *Philos. Mag. B* **1982**, *46*, 137. (b) Burian, A.; Lecante, P.; Mosset, A.; Galy, J. *J. Non-Cryst. Solids* **1987**, *90*, 633. (c) Laberty, C.; Verelst, M.; Lecante, P.; Mosset, A.; Alphonse, P.; Rousset, A. *J. Solid State Chem.* **1997**, *129*, 271. (d) Verelst, M.; Sommier, L.; Lecante, P.; Mosset, A.; Kahn, O. *Chem. Mater*. **1998**, *10*, 980. (e) Cador, O.; Mathonière, C.; Kahn, O.; Costes, J.-P.; Verelst, M.; Lecante, P. *Inorg. Chem.* **1999**, *38*, 2643.
(18) The CERIUS2 molecular simulation program is supplied by BIOSYM technologies and runs on an Indy Silicon Graphics workstation.
(19) Debye, P. *Ann. Phys. (Leipzig)*, **1915**, *46*, 809.

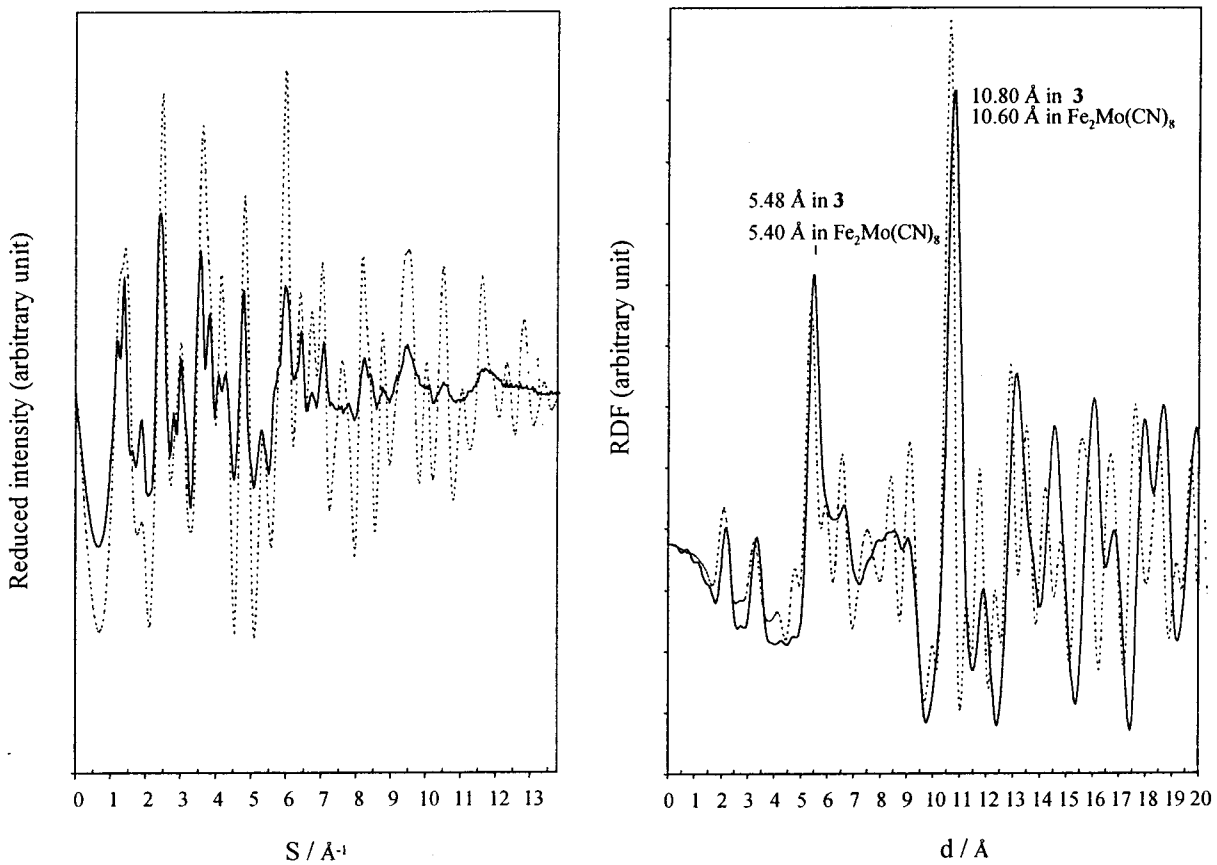

Figure 3. Reduced intensity (left) and RDF (right) calculated from experimental data for $Mn^{II}_2[Mo^{IV}(CN)_8]\cdot 9.5H_2O$ (**3**) (−) compared to those calculated from structural data given for $Fe^{II}_2(H_2O)_4[Mo^{IV}(CN)_8]\cdot 4H_2O$ (- - -).

Table 2. Selected Bond Lengths (Å) and Angles (deg) for **1**[a]

Mo(1)−C(41)	2.136(5)	Cu(1)−N(4)	1.986(4)
Mo(1)−C(42)	2.149(5)	Cu(1)−N(1)	1.994(4)
Mo(1)−C(45)	2.151(6)	Cu(1)−N(3)	2.042(4)
Mo(1)−C(48)	2.151(6)	Cu(1)−N(2)	2.153(5)
Mo(1)−C(43)	2.162(6)	Cu(2)−N(10)	1.973(4)
Mo(1)−C(44)	2.161(5)	Cu(2)−N(8)	1.988(5)
Mo(1)−C(47)	2.170(6)	Cu(2)−N(5)	1.992(5)
Mo(1)−C(46)	2.178(5)	Cu(2)−N(7)	2.061(5)
Cu(1)−N(9)	1.963(4)	Cu(2)−N(6)	2.105(5)
Cu1−Cu2	9.795(1)	O1W−O5W^{ii}	2.761(11)
Cu1−Mo1	5.1625(7)	O1W−O5W^{iii}	2.923(13)
Mo1−Cu2	5.2325(8)	O1W−O2W	2.832(9)
N11−O3W	2.929(9)	O3W−O4W^{iv}	2.903(13)
N12−O1W^{i}	2.783(7)	Cu1−Cu1^{v}	6.2241(13)
N14−O2W	2.985(10)	Cu1−Mo1	5.1625(7)
N15−O4W	2.96(1)		
Cu(1)−N(9)−C(41)	161.3(4)	C(42)−N(10)−Cu(2)	166.6(5)
N(9)−C(41)−Mo(1)	175.4(4)	N(4)−Cu(1)−N(1)	174.04(18)
C(41)−Mo(1)−C(42)	144.6(2)	N(8)−Cu(2)−N(5)	172.5(2)
Mo(1)−C(42)−N(10)	178.0(5)		

[a] Symmetry transformation used to generate equivalent atoms: (i) $x-1, y+1, z$; (ii) $x+1, -y+1, -z+1$; (iii) $x, y-1, z$; (iv) $x+1, y, z$; (vi) $-x, -y+1, -z+1$.

distances are probably due to the formation of hydrogen bonds. In fact, they are very similar to those obtained in $[Pt(NH_3)_4]_2[W(CN)_8][NO_3]\cdot 2H_2O$ where the hydrogen-bonding network is evident from the location of the hydrogen atoms.[20] The shortest copper−copper distance is between two fragments, with Cu1−Cu1 = 6.224(1) Å.

WAXS Study of $M_2[Mo(CN)_8]\cdot xH_2O$. Figure 3 shows the reduced intensities and the RDF for $Mn_2[Mo(CN)_8]\cdot 9.5H_2O$ (**3**) compared to those calculated from structural data of $Fe^{II}_2(H_2O)_4[Mo^{IV}(CN)_8]\cdot 4H_2O$.[10] The reduced intensity represents the structural part of the scattering phenomenon after the full correction procedure. The Fourier transform of this spectrum gives the RDF, which can be considered as a histogram of ordered distances weighted by the distance multiplicity and the number of electrons engaged in these distances. Thus, an intense peak on the RDF indicates a frequent occurrence of distance between two heavy atoms.

Clearly, this WAXS investigation indicates that **3** has an architecture similar to that of $Fe^{II}_2(H_2O)_4[Mo^{IV}(CN)_8]\cdot 4H_2O$ because the experimental reduced intensity and RDF for **3** fit very well those calculated for $Fe^{II}_2(H_2O)_4[Mo^{IV}(CN)_8]\cdot 4H_2O$. Only a small discrepancy is detected in the first M−Mo distance, which is found to be equal to 5.48 Å in the manganous compound and 5.40 Å in the ferrous compound. The main Mo−Mo distances are found to be 10.80 Å (Mn compound) and 10.60 Å (Fe compound). Other Mo−Mo distances in the structure of $Fe^{II}_2(H_2O)_4[Mo^{IV}(CN)_8]\cdot 4H_2O$ (6.55 and 8.35 Å) give weak peaks in the RDF and are difficult to assign clearly. We conclude that **3** has the same network as $Fe^{II}_2(H_2O)_4[Mo^{IV}(CN)_8]\cdot 4H_2O$ and is slightly larger according to the bigger size of Mn^{2+} (0.91 Å) compared to the size of Fe^{2+} (0.82 Å).

The case of **2** is more complicated. Indeed, the reduced intensity and RDF of **2** shown in Figure 4 do not properly fit those calculated for $Fe^{II}_2(H_2O)_4[Mo^{IV}(CN)_8]\cdot 4H_2O$. Therefore, these two compounds do not have the same structure. However, a qualitative look shows that up to 6 Å both RDFs indicate some analogies indicating a close Mo−CN−M core. But the Mo···Cu distance found at 5.25 Å seems to be sensibly shorter than in other compounds of this family. Assuming that the second intense peak is due to the main Mo···Mo distance for **2**, this distance is found to be 10.15 Å, which is quite shorter

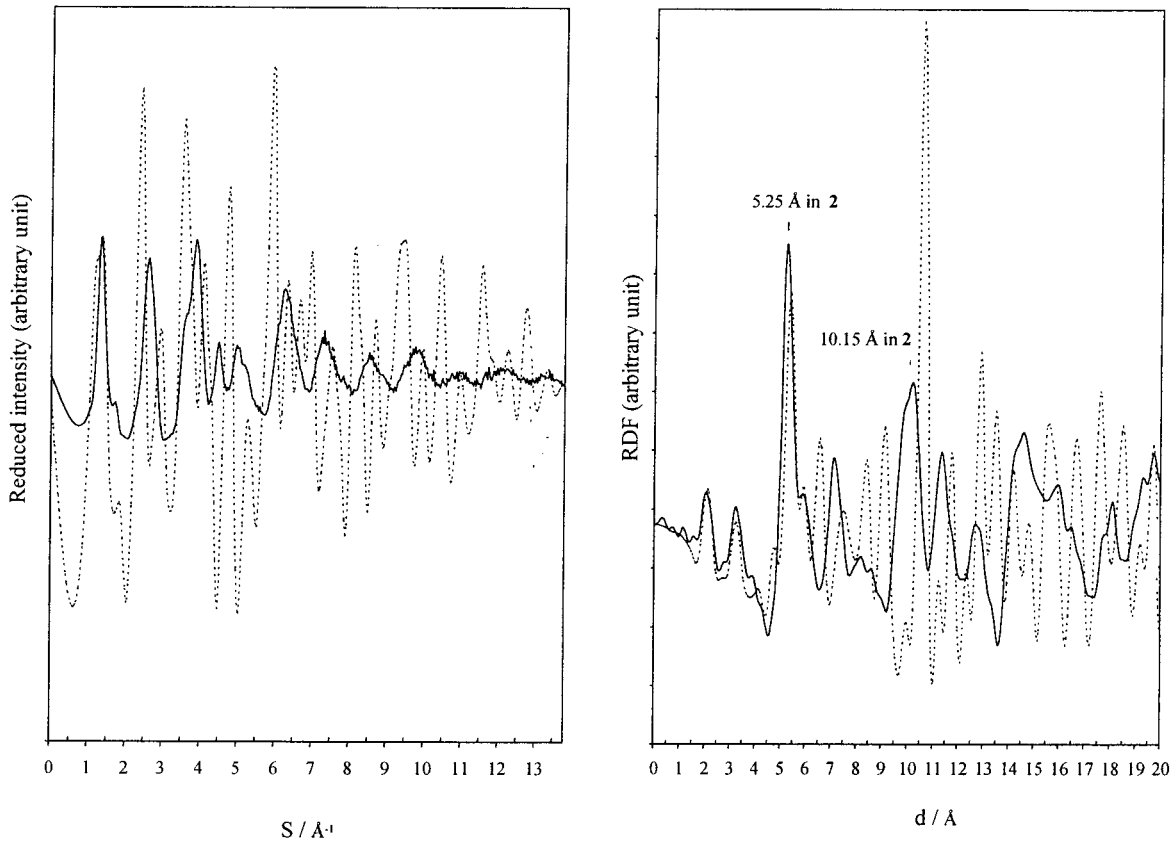

Figure 4. Reduced intensity (left) and RDF (right) calculated from experimental data for $Cu^{II}_2[Mo^{IV}(CN)_8]\cdot 7.5H_2O$ (**2**) (−) compared to those calculated from structural data given for $Fe^{II}_2(H_2O)_4[Mo^{IV}(CN)_8]\cdot 4H_2O$ (- - -).

than that found in other compounds. This characteristic is once more in agreement with the smaller ionic radius of Cu^{2+} (0.72 Å) compared with those of Mn^{2+} and Fe^{2+} ions and could be reproduced by a reduction (×0.97) of cell parameters of $Fe^{II}_2(H_2O)_4[Mo^{IV}(CN)_8]\cdot 4H_2O$. What strongly differs in $Fe^{II}_2(H_2O)_4[Mo^{IV}(CN)_8]\cdot 4H_2O$ and **2** is the 6−10 Å area, which mainly represents M−M distances rather than Mo−M distances. These discrepancies cannot be resolved simply by applying the reduction factor of cell parameters. This clearly indicates that the structural arrangement around the metallic cores is different in the two compounds.

To simulate the structure of **2**, two hypotheses for the coordination geometry of copper have been tried, namely, a perfect square planar (D_{4h} symmetry) geometry and a perfect tetrahedron (T_d symmetry). For both models, the molybdenum coordination geometry has been adjusted in order to generate a set of Cu···Cu distances: the first one at 6 Å and the second one at 7.15 Å. Both simulations have been compared with experimental data in Figure 5 (left, reduced intensity; right, RDF). On one hand, the tetrahedral geometry around the copper ion is not adapted because it generates Mo···Mo distances close to 8.95 Å, which are clearly too short. On the other hand, the square planar geometry leads to an Mo···Mo distance equal to 10.35 Å, which is rather close to 10.15 Å found experimentally. The fitting quality between the square planar model and the experimental data (both reduced intensity and RDF) is reasonably good for considering this hypothesis a good model for **2**.

The simulated model does not fit perfectly the experimental data because the eight water molecules have not been included. In particular, it is impossible from a WAXS study to distinguish between a square planar geometry (i.e., four-coordinate sphere) or a strongly distorded octahedral geometry with two water molecules in apical positions (i.e., (4 + 2)-coordinate sphere). Both geometries are of D_{4h} symmetry, and to fully describe the coordination sphere around the Cu ion, XANES and EXAFS studies are in progress. However, for our purpose in this paper, we can conclude that **2** and $Fe^{II}_2(H_2O)_4[Mo^{IV}(CN)_8]\cdot 4H_2O$ are three-dimensional networks with similar Mo−CN−M cores.

Magnetic and Photomagnetic Properties of $[Cu(bipy)_2]_2[Mo(CN)_8]\cdot 5H_2O\cdot CH_3OH$ (1) and $Cu_2[Mo(CN)_8]\cdot 7.5H_2O$ (2). In this section, we will present first the magnetic and photoinduced magnetic properties of **1** and then those obtained for **2**. Both compounds have optical absorptions in the UV range corresponding to ligand-field bands of the $Mo(CN)_8^{4-}$ chromophore. **2** exhibits also an intense band around 500 nm corresponding to an intervalence charge transfer (IVCT) corresponding to $Cu^{II}-Mo^{IV} \rightarrow Cu^{I}-Mo^{V}$. Therefore, visible and UV ranges were used for irradiation.

Before irradiation, the magnetic properties of **1** were simply measured as the field dependence of the magnetization M at 10 K (Figure 6) because no magnetic interactions are expected of this trinuclear molecule formed by two Cu^{II} ions ($S_{Cu} = {}^1/_2$) separated by the diamagnetic Mo^{IV} ion ($S_{Mo} = 0$). The curve corresponds to what is expected for two paramagnetic Cu ions and fits perfectly the Brillouin function for two noninteracting $S = {}^1/_2$ spins. Under UV irradiation at 10 K, the magnetization of **1** at 10 kOe increased rapidly and slowly reached saturation (see inset in Figure 6). The light was turned off after 15 h of irradiation, and the photoinduced magnetization was observed to be stable. Then the field dependence of the magnetization after irradiation was measured at 10 K (Figure 6). The curve obtained after irradiation is above the curve obtained before irradiation, which indicates that the system is more magnetic. To obtain further information on the photogenerated state, the

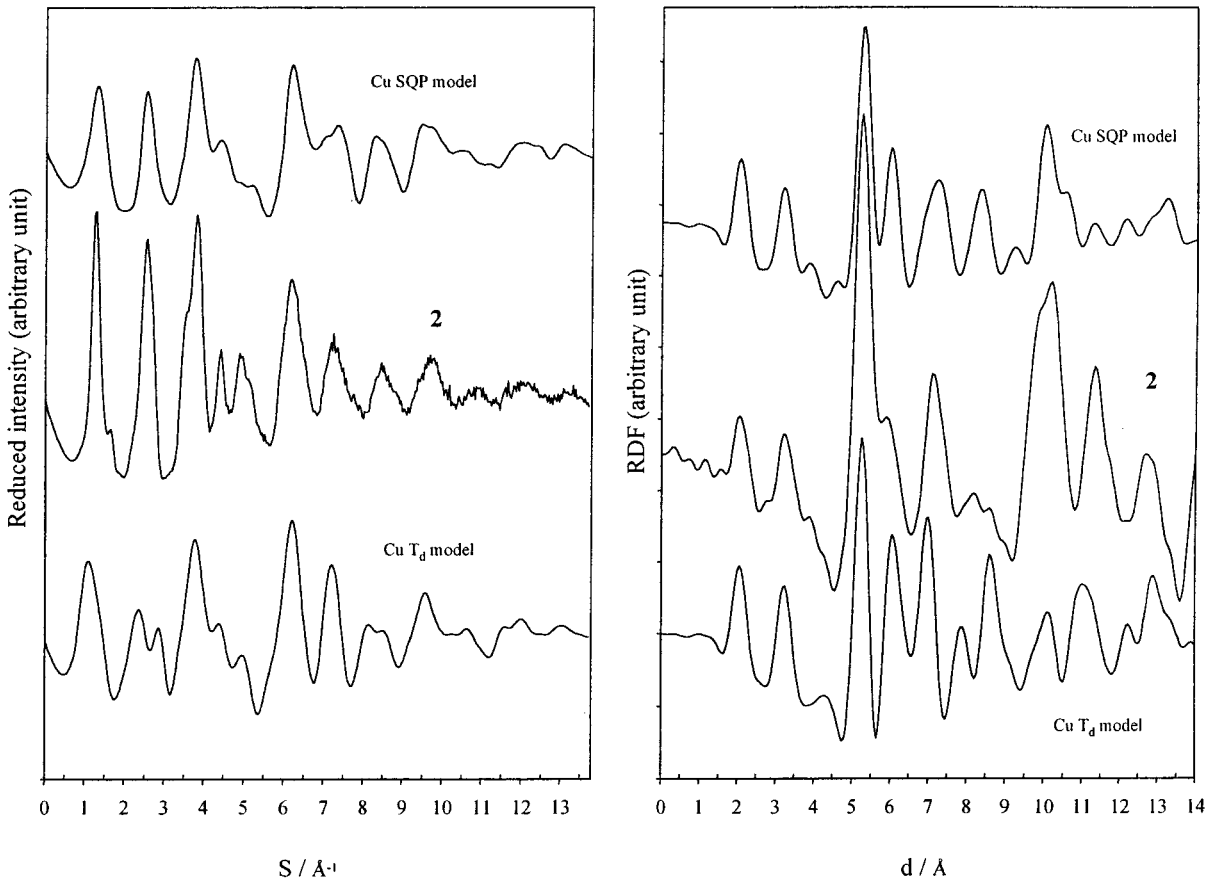

Figure 5. Reduced intensity (left) and RDF (right) calculated from experimental data for $Cu^{II}_2[Mo^{IV}(CN)_8]\cdot 7.5H_2O$ (**2**) compared to those calculated from models (see text).

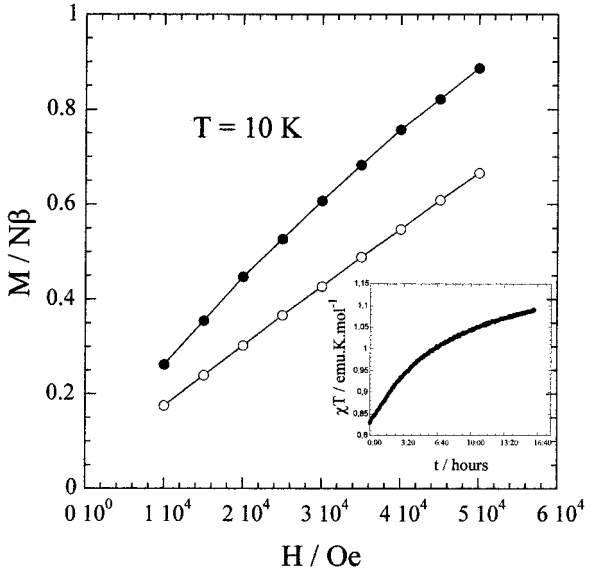

Figure 6. Field dependence of the magnetization M at 10 K for $[Cu(bipy)_2]_2[Mo(CN)_8]\cdot 5H_2O\cdot CH_3OH$ (**1**) before (○) and after (●) UV irradiation. The inset shows the time dependence of the magnetization under irradiation. The full lines are only guides for the eye.

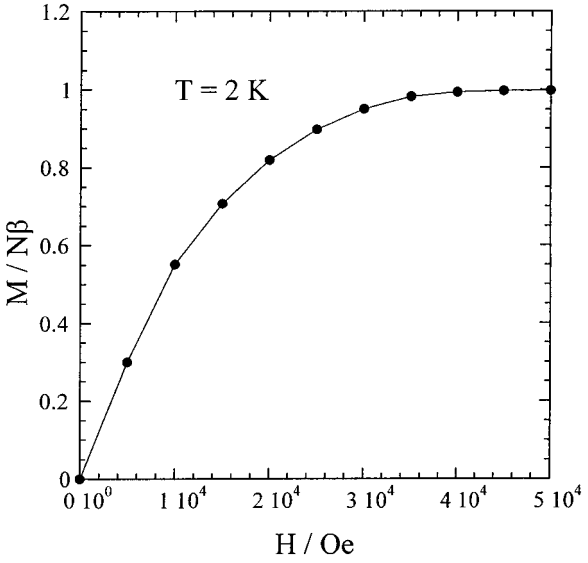

Figure 7. Field dependence of the magnetization M at 2 K for $[Cu(bipy)_2]_2[Mo(CN)_8]\cdot 5H_2O$ (**1**) after UV irradiation. The full lines are only guides for the eye.

magnetization has been recorded at 2 K, as displayed on Figure 7. A saturation value of 1 $N\beta$ is reached with an external field of 50 kOe. Finally the $\chi_M T$ vs T curve, χ_M being the molar magnetic susceptibility and T the temperature, was recorded in warming mode in the 2−200 K under a magnetic field of 10 kOe. The curve is shown in Figure 8. At low temperature the curve increases from 0.86 emu K mol^{-1} to near 70 K 1.16 emu K mol^{-1}. This value is maintained until room temperature. This value is in very good agreement with the calculated value of 1.125 emu K mol^{-1} for three isolated $S = {}^1/_2$ spins and $g = 2$. The decrease of the $\chi_M T$ product at low temperature is indicative of antiferromagnetic interactions. These data may be interpreted by considering three antiferromagnetically coupled $S = {}^1/_2$ spins. By use of the spin Hamiltonian $\hat{H} = -J\,(\hat{S}_{Cu1}\hat{S}_{Mo} + \hat{S}_{Cu2}\hat{S}_{Mo})$, S being the spin operator for each ion and J the interaction

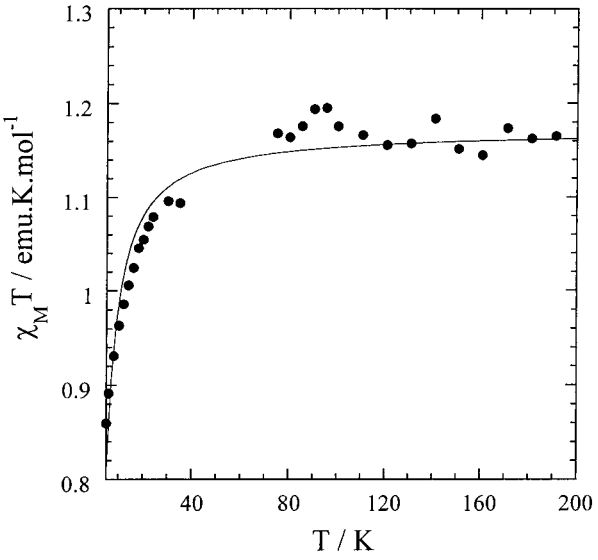

Figure 8. Experimental (●) and calculated (−) $\chi_M T$ vs T plot for $[Cu(bipy)_2]_2[Mo(CN)_8]\cdot 5H_2O\cdot CH_3OH$ (**1**) after UV irradiation. The points in the 35−70 K range were deleted because of oxygen absorption by the sample.

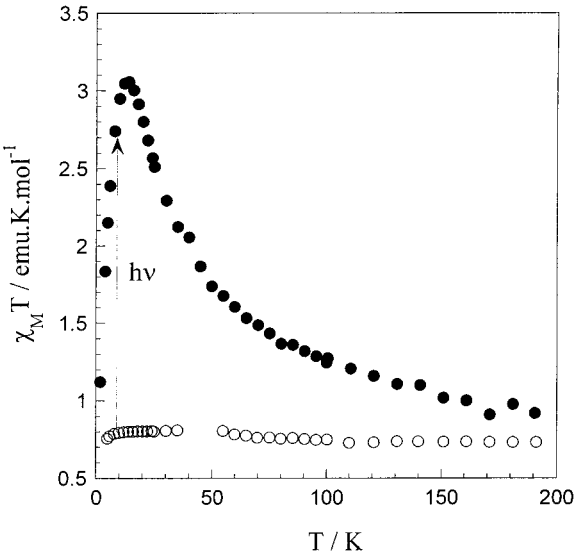

Figure 9. $\chi_M T$ vs T plot before (○) and after (●) irradiation for $Cu^{II}_2[Mo^{IV}(CN)_8]\cdot 7.5H_2O$ (**2**). The points in the 35−70 K range were deleted because of oxygen absorption by the sample.

parameter between the terminal Cu ions and the central Mo ion, the theoretical expression of $\chi_M T$ is then given by

$$\chi_M T = \frac{N\beta^2 g^2}{4k} \frac{1 + \exp\left(\frac{J}{kT}\right) + 10\exp\left(\frac{3J}{2kT}\right)}{1 + \exp\left(\frac{J}{kT}\right) + 2\exp\left(\frac{3J}{2kT}\right)} \qquad (1)$$

The fitting of the experimental data led to $J = -3.18$ cm^{-1} and $g = 2.04$. This J value confirms weak antiferromagnetic interactions in the photogenerated system. The photoinduced magnetic behavior is maintained after cycling the temperature, 2−300−2 K. Hence, the UV irradiation provokes irreversible change of compound **1**. In contrast, irradiation with visible light does not lead to modifications of magnetic behavior.

The magnetic properties of **2** have been recorded as the $\chi_M T$ vs T and M vs H curves. These two curves are displayed in Figures 9 and 10, respectively. The $\chi_M T$ value at room temperature is equal to 0.78 emu K mol^{-1}, which is close to

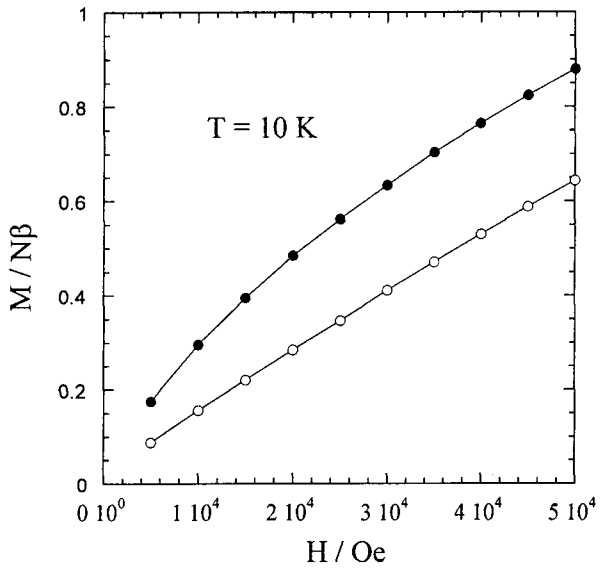

Figure 10. Field dependence of the magnetization M at 10 K for $Cu^{II}_2[Mo^{IV}(CN)_8]\cdot 7.5H_2O$ (**2**) before (○) and after (●) UV irradiation. The full lines are only guides for the eye.

the expected value of 0.75 emu K mol^{-1} for two $S = {}^1/_2$ spins and $g = 2$. When T decreases, the $\chi_M T$ value is constant until 10 K, and then it decreases. This is indicative of very weak antiferromagnetic interactions. Similar behavior has been observed for **3** and $Fe^{II}_2(H_2O)_4[Mo^{IV}(CN)_8]\cdot 4H_2O$.[10] For **3** the antiferromagnetic interactions are found to be a little bit stronger and are interpreted to take place through the $NC-Mo^{IV}-CN$ diamagnetic spacer. In the case of $Fe^{II}_2(H_2O)_4[Mo^{IV}(CN)_8]\cdot 4H_2O$, the decrease of $\chi_M T = f(T)$ is due to the combined effects of antiferromagnetic interactions and spin−orbit coupling.

The magnetic properties of **2** can be modified under UV or visible light. Similar magnetic curves after irradiation are obtained. The main difference is that the time dependence of the increase of the magnetization under visible light is slower than that obtained under UV light. In the following we will present the case of visible irradiation. Under visible light irradiation at 10 K, the magnetization of **2** increased rapidly and slowly reached saturation. The light was turned off after 12 h of irradiation, and the photoinduced magnetization was observed to be stable. Then the field dependence of the magnetization after irradiation was measured at 10 K (Figure 10). As observed for **1**, the curve obtained after irradiation is above the curve before irradiation, which indicates that the system is more magnetic. Then the magnetization at 2 K was measured and showed a value of 1.7 $N\beta$ with an external field of 50 kOe. More informative is the $\chi_M T$ vs T curve obtained in warming mode. At very low temperature, the curve increases, reaching a maximum of 3.10 emu K mol^{-1} at 15 K, then rapidly decreases until 200 K to a value of 0.89 emu K mol^{-1}. We checked that the maximum observed is not due to relaxation processes by recording in the dark for 1 h the $\chi_M T$ products at 5 K and then at 25 K, and both are found to be stable. As mentioned in the Experimental Section, the uncertainty in the data above 200 K is not negligible and it is not possible from the $\chi_M T$ plot to know accurately the temperature when the modifications by light irradiation are erased. But interestingly the $\chi_M T$ value at 10 K obtained after warming the sample at room temperature is 0.72 emu K mol^{-1}, which corresponds approximately to the value observed before irradiation. This shows that the modifications of magnetic properties under visible or UV irradiation are reversible with a thermal treatment.

Discussion

The two compounds presented in this paper exhibit photoinduced magnetic modifications under light perturbation in the solid state. Therefore, they are new examples of molecular photomagnetic systems. In fact, such systems are not so numerous. To the best of our knowledge, the Fe^{II} spin crossover compounds,[21] the hexacyanometalates mentioned in the Introduction, and the photochemical generation of triplet carbene centers from diazo groups[22] are the only cases reported so far with metal ions. More recently, a photoswitching of intramolecular magnetic interactions using a photochromic unit of a thiophene derivative with closed- or open-ring isomers formed by light irradiation has been demonstrated.[23] It seemed to us important to find out about other photomagnetic examples in the field of molecular materials. The use of a photosensitive metallic building block is interesting because new mixed-metal compounds can be designed. Moreover, this work shows that different behaviors of magnetic modifications can be generated under light irradiation.

Before a discussion of the possible mechanisms of photomagnetic effects in **1** and **2**, let us recall their main differences. The photoinduced magnetic behavior in **1** is obtained only with UV irradiation and is not thermally reversible. For **2**, similar photomagnetic effects are obtained under UV or visible irradiation but with different kinetics, and in these two cases, they are thermally reversible. These distinct features of **1** and **2** helped us to propose mechanisms for explaining the observed behaviors.

The photomagnetic properties of **1** results from a photooxidation of Mo^{IV} to Mo^{V}. This is proposed from a comparison of results obtained recently on the one-dimensional chain $[Mn^{II}_2(Mac)_2(H_2O)][Mo^{IV}(CN)_8]\cdot 5H_2O$.[6] This photooxidation is probably accompanied by a reduction of at least one water molecule in OH^- and $(^1/_2)H_2$, making the phenomenon irreversible. This requires the vicinity of at least one H_2O molecule in the molybdenum surrounding in the structure. Both $[Mn^{II}_2(Mac)_2(H_2O)][Mo^{IV}(CN)_8]\cdot 5H_2O$ and **1** exhibit short distances between nonbridging cyano groups and oxygen atoms of noncoordinated water molecules as given in Figure 2 and Table 2. Therefore, the initial system being the trinuclear triad $Cu^{II}(S = {}^1/_2)-Mo^{IV}(S = 0)-Cu^{II}(S = {}^1/_2)$ becomes, under irradiation, the triad $Cu^{II}(S = {}^1/_2)-Mo^{V}(S = {}^1/_2)-Cu^{II}(S = {}^1/_2)$. This is supported by the $\chi_M T$ value obtained at high temperature. In the photogenerated state, the creation of the magnetic site in the middle of the triad leads to antiferromagnetic interactions between the two copper ions. The J value deduced from a comparison between data and theory is in agreement with values found in other bimetallic cyanide compounds.[24] The saturation value obtained for the magnetization at 2 K at 1 $N\beta$ is consistent with a total spin $S = {}^1/_2$ coming from an antiferromagnetic interaction between terminal Cu ions and Mo ion.

This photooxidation is not possible for **2**. In fact, the combination of IR spectroscopy (one peak in the CN stretching region) and the WAXS analysis shows that all the cyano groups are involved in coordination with Cu sites, as found in $Fe^{II}_2(H_2O)_4[Mo^{IV}(CN)_8]\cdot 4H_2O$. This means that no water molecules are close to the Mo ion. The electron transfer occurs between Mo^{IV} and Cu^{II}, as anticipated with the optical spectrum. This leads to the formation of $Mo^{V}-Cu^{I}$ pairs in the material. This mechanism of induced electron transfer is similar to what has been observed in Hashimoto's compounds. Actually, the mechanism involves the formation of a Cu^{I} site, which is known to adopt mostly linear, trigonal planar, or tetrahedral geometries rather than D_{4h} symmetry. After photoexcitation, the system is trapped in a metastable state noted as $(Mo^{V}-CN-Cu^{I})_M$ where a structural distortion may occur in the Cu surroundings. This reorganization would imply, in the case of the CuN_4 unit, a rotation around a 2-fold axis to form an intermediate geometry between D_{4h} and T_d symmetries. In the case of a (4 + 2)-coordinate sphere, the CuN_4O_2 unit would go through elongations of Cu−O bonds and rotation around Cu. Such a mechanism is in agreement with the IVCT excitation in the visible range. When the system is irradiated in the UV range, the excited state is different but relaxes toward the same metastable state $(Mo^{V}-CN-Cu^{I})_M$. The IVCT photoexcitation may be summarized through the following scheme:

$$Mo^{IV}-CN-Cu^{II} \xrightarrow{IVCT} (Mo^{V}-CN-Cu^{I})^* \rightarrow (Mo^{V}-CN-Cu^{I})_M$$

The thermal reversibility of the phenomenon is due to the back electron transfer through an energy barrier, leading to the thermal depopulation of the metastable state. Now to explain the inefficiency of the visible photoexcitation for **1**, we may argue that the proposed structural reorganization of the five-coordinate Cu spheres would occur with the breaking of one Cu−N bond, which is not compatible with the energy provided by the illumination and the chelate effect of the 2,2′-bipyridine ligand. Therefore, the only available process for **1** is the photooxidation mechanism.

If we assume that the photoinduced electron transfer is nearly quantitative for **2**, the photogenerated system should have a formula close to $Cu^{II}Cu^{I}[Mo^{V}(CN)_8]\cdot 4H_2O$. Since the Cu^{I} ($3d^{10}$) is diamagnetic, the irradiation leads to the creation of an $S = {}^1/_2$ spin for Mo but also the loss of $S = {}^1/_2$ for Cu. This means that irradiation does not create spins; it creates a different localization of the magnetic centers. The low-field values of M, which are significantly higher than the nonirradiated curve, reveal that exchange interactions are ferromagnetic between Cu^{II} and Mo^{V} centers. However, they do not lead to magnetic ordering, maybe because of the presence of diamagnetic Cu^{I} ions cutting off magnetic interaction pathways and/or irradiation exposition (time and power) not being sufficient to convert all the $Mo^{IV}-Cu^{II}$ pairs. The maximum observed in the $\chi_M T$ vs T curve at 15 K is due to magnetic phenomena. Such maxima of $\chi_M T$ have already been observed in high-spin clusters or chains, and they are due to antiferromagnetic intercluster interactions or zero-field splitting. In our case, the formation of clusters with dominant ferromagnetic interactions alternating Mo^{V} and Cu^{II} with small antiferromagnetic intercluster (or chain) interactions is in agreement with the $\chi_M T$ vs T curve in the low-temperature range.

This study shows that exchange interactions between Cu^{II} and photogenerated Mo^{V} can be antiferromagnetic in a trinuclear bent molecule and ferromagnetic in a 3D network. In the case of compound **2**, the ferromagnetism may be due to electron delocalization that could favor parallel alignment of spins. To

(20) Siekluka, B.; Lasocha, W.; Proniewicz, L. M.; Podgagny, R.; Schenk, H. *J. Mol. Struct.* **2000**, *520*, 155.
(21) (a) Hauser, A. *Coord. Chem. Rev.* **1991**, *111*, 275. (b) Létard, J.-F.; Capes, L.; Chastanet, G.; Moliner, N.; Létard, S.; Real, J. A.; Kahn, O. *Chem. Phys. Lett.* **1999**, *313*, 115.
(22) (a) Sano, Y.; Tanaka, Y.; Koga, N.; Matsuda, K.; Iwamura, H.; Rabu, P.; Drillon, M. *J. Am. Chem. Soc.* **1997**, *119*, 8246. (b) Karasawa, S.; Sano, Y.; Akita, S.; Koga, N.; Itoh, T.; Iwamura, H.; Rabu, P.; Drillon, M. *J. Am. Chem. Soc.* **1998**, *120*, 10080.
(23) Matsuda, K.; Irie, M. *J. Am. Chem. Soc.* **2000**, *122*, 8309.
(24) (a) Scuiller, A.; Mallah, T.; Verdaguer, M.; Nivorozkhin, J. L. *New J. Chem.* **1996**, *20*, 1. (b) Miyasaka, H.; Ieda, H.; Matsumoto, N.; Re, N.; Crescenzi, F. C. *Inorg. Chem.* **1998**, *37*, 255. (c) Langenberger, K. V.; Batten, S. R.; Berry, K. J.; Hockless, D. C. R.; Mourabaki, B.; Murray, K. S. *Inorg. Chem.* **1997**, *36*, 5006.

rationalize these results, better knowledge of the structure of the photogenerated compound is necessary. We are now engaged in WAXS, XANES, and EXAFS studies under light irradiation.

Conclusion

The reaction of the photosensitive building block $Mo^{IV}(CN)_8^{4-}$ with Cu^{2+} allowed us to prepare several bimetallic compounds, from finite molecules to extended networks. These compounds display two different kinds of photomagnetic effects. The first is based on a chemical reaction (photooxidation in our case) between a metallic center (here the Mo^{IV} ion) and solvent molecules present in the structure. We have shown that this type of reaction is maintained in the solid state and at low temperatures and can lead to irreversible photomagnetic behavior. The second effect results from a photoinduced electron transfer between two different metallic centers. The modification of the magnetic properties is reversible, and our compound is another example of a switchable molecular spin device. In the future, we hope to report further studies of these particular compounds to elucidate the origin and the mechanisms of the thermal relaxations.

Supporting Information Available: An X-ray crystallographic file, in CIF format, for the structure determination of compound **1**. This material is available free of charge via the Internet at http://pubs.acs.org.

IC0008722